We are IntechOpen, the world's leading publisher of Open Access books Built by scientists, for scientists

6,900
Open access books available

185,000
International authors and editors

200M
Downloads

Our authors are among the

154
Countries delivered to

TOP 1%
most cited scientists

12.2%
Contributors from top 500 universities

WEB OF SCIENCE™

Selection of our books indexed in the Book Citation Index in Web of Science™ Core Collection (BKCI)

Interested in publishing with us?
Contact book.department@intechopen.com

Numbers displayed above are based on latest data collected.
For more information visit www.intechopen.com

Chapter 6

Thermoelectric Devices: Influence of the Legs Geometry and Parasitic Contact Resistances on ZT

Angel Fabiam-Mijangos and
Jaime Alvarez-Quintana

Additional information is available at the end of the chapter

http://dx.doi.org/10.5772/intechopen.75790

Abstract

In this chapter, the impact of the shape of thermoelectric legs and parasitic contact resistances from metal electrodes and device wiring on thermoelectric figure of merit ZT is addressed. First section deals with the influence of the legs geometry on ZT. The shape of the legs is crucial in the thermoelectric performance of the thermoelectric devices. Unlike to conventional geometry thermoelectric legs, non-constant cross-section legs could help by lowering the overall thermal conductance of the device so as to increase the temperature gradient along legs, hence harnessing the Thomson effect, which is generally neglected in constant square cross-section thermoelectric legs. The final section is devoted to the electrical contact engineering of the device. Parasitic contact and wiring resistances play an important role in the performance of the device because they increase the isothermal resistance of the device. As the isothermal resistance of the device increases, the ZT decreases.

Keywords: asymmetrical legs, energy harvesting, heat recovery, heat recycling, thermoelectric module

1. Introduction

Waste heat occurs in many areas of daily life (natural and industrial processes). In general, generation of 1 W of power using the state-of-the art heat engines requires about 3 W of energy input, which results in dumping into the environment the equivalent of about 2 W of power in the form of heat. Thereby, waste heat recovery to create a source of energy is an important technology for a stable supply of electricity and environmental protection. In particular, the heat loss due to low temperature, which is below 450 K, represents a large portion of waste heat emitted from an automobile and industry. For instance, in the US manufacturing sector

IntechOpen

© 2018 The Author(s). Licensee IntechOpen. This chapter is distributed under the terms of the Creative Commons Attribution License (http://creativecommons.org/licenses/by/3.0), which permits unrestricted use, distribution, and reproduction in any medium, provided the original work is properly cited. CC BY

alone, more than 3000 TW of waste heat energy is lost each year, an amount equivalent to more than 1.72 billion barrels of oil [1]. Hence, efficiently reclaiming even a small portion of such waste heat would itself nearly satisfy the electricity needs of the planet [2]. Thermoelectricity enabling directly converting heat into electricity using thermoelectric converters is a promising energy technology, which is under intense research to provide a solution to thermal energy recovery and management. However, wide-scale applications of this technology are limited due to the relative low thermoelectric efficiency of current materials and devices. For this reason, thermoelectric technology is only used in niche applications where its solid-state nature outweighs its poor efficiency. Therefore, an attractive and sustainable solution to the energy problem would be the development of solid-state thermoelectric devices which could help to recover this waste heat efficiently. The performance of a thermoelectric material is evaluated by the dimensionless figure of merit, *ZT*, which is defined as $ZT = S^2\sigma T/k$, where σ is the electrical conductivity, *S* is the Seebeck coefficient (i.e. thermopower), *k* is the thermal conductivity (often separated into the lattice thermal conductivity, k_L, and the carrier thermal conductivity, k_e), and *T* is the absolute temperature [3]. Good thermoelectric materials must have a high Seebeck coefficient to have high voltage output, low electrical resistivity to minimize Joule heating and low thermal conductivity to sustain large temperature gradients [4]. Clearly, the enhancement of *ZT* is not an easy task because these physical parameters are interdependent, and an improvement in one of these properties affects adversely another one. Hence, the development of high-efficiency thermoelectric materials and systems is very challenging. For instance, at material level recent developments in nanotechnology have led significant *ZT* enhancements in two-dimensional (thin films) and one-dimensional (nanowires, nanorods, nanotubes, etc.) thermoelectric materials [4–12]. In any case, although both strategies at nanoscale seems to be promising so as to increase *ZT* at material level, the main constraint for real applications is related to the tiny size of such nanostructures. Evidently, low-dimensional thermoelectric materials have limited applications for large-scale energy-conversion, because they are too thin to support appreciable temperature differentials [13–15]. In this sense, due to this disadvantage, researchers have been extensively focused on nanocomposites to perform nanoscale thermoelectric enhancement in bulk thermoelectric materials [13, 16–20].

On the other hand, at device level evidently the transfer from material to device affects significantly the intrinsic figure of merit of the material; hence the different materials and substrates constituting the thermoelectric device as well as its architecture play an important role in the thermoelectric figure of merit of the device, as consequence, an effective thermoelectric figure of merit lower than the intrinsic one could be presented in the thermoelectric module [21]. In this sense, significant enhancements in *ZT* by nanostructuring bulk materials could be seriously affected because of deficiencies during the design of thermoelectric devices. In the past, several strategies have been developed in order to improve the thermoelectric performance at device level, such strategies include filling of the empty space between thermoelectric legs with silica aerogel to minimize the thermal shunt path [22], improvement of the electrical and thermal contact between thermoelectric legs and refractory materials by using a buffer layer of carbon and Ni-Ag- based brazing material [23], even the use of thermoelectric legs modified with an organic layer has been proposed to improve the electrical contact resistance [24]. Besides, a theoretical study has proposed the cascade architectures that

combine two or more thermoelectric modules with different working temperature range in order to increase the output power of the device [25], the heat-shrink type where the module has a cross-plane heat transfer architecture similar to a conventional bulk TE module, but with heat transfer in the plane of the thin film thermoelectric elements, which assists in maintaining a significant temperature difference across the thermoelectric junctions [26], and the planar type where the thermoelectric legs are patterned onto the surface of a dielectric substrate [27, 28]. A complete review of the approaches used to enhance the thermoelectric performance in materials and devices is beyond of the scope of the present chapter; nevertheless, to explore about the strategies previously and currently proposed at the material and device level, the in-depth review can be found in the literature [29–31].

Evidently, the performance of thermoelectric devices depends on many factors, such as the temperature difference between hot and cold plates, thermoelectric legs and device material properties, as well as the configuration and arrangement of thermoelectric legs. Among these factors, the geometry and configuration of the thermoelectric legs are crucial. In this sense, several studies under a purely theoretical context have predicted the effects of varying the geometry of the legs on the thermoelectric performance of the device. For instance, it has been reported that a smaller number of shorter legs have the potential to achieve the same power per unit module area as a greater number of longer legs [32]. It has also been studied that the effect of the number of legs and their heights on the maximum output power and efficiency of the thermoelectric generator in order to find the optimum arrangements of legs [33]. Moreover, it has been analyzed that the thermoelectric performance of the device by variations in the cross-section of the legs (legs with non-constant cross sections), and predictions show that legs with trapezoid legs (linear variation cross-section) have higher nominal power density than quadratic and exponential variations in cross-sectional legs [34, 35]. In addition, the tailoring of the geometry configuration of the legs in line with the device operating conditions has also been analyzed via thermoelectric legs tapering [36], as well as the thermoelectric performance of thermoelectric generators and coolers in relation to the geometry of non-constant cross-section legs has been formulated thermodynamically [37], and via genetic algorithms [38–40] for pyramid, cylindrical, and cuboid shapes with the aim of accomplishing device geometric optimization.

As mentioned above, the design and optimization of thermoelectric legs have previously been studied theoretically. However, experimental work confirming these theoretical predictions has not been carried out so far, mainly because of the difficulties involving in fabrication of thermoelectric legs with complex geometrical structures. Section 2 of the present chapter deals with the influence of the legs geometry on ZT. Unlike conventional geometry thermoelectric legs, non-constant cross-section legs could help by lowering the overall thermal conductance of the device so as to increase the temperature gradient along legs, hence harnessing the Thomson effect, which is generally neglected in constant square cross-section thermoelectric legs as it shows a complete theoretical and experimental analysis of asymmetrical legs. Section 3 is devoted to the electrical contact engineering of the device. Parasitic contact and wiring resistances play an important role in the performance of the device because they increase the isothermal resistance of the device. Finally, in Section 4, conclusions about of the results presented in this chapter are shown.

2. Theoretical and experimental analysis of symmetrical and asymmetrical legs

According to previous theoretical studies, the investigation of the geometric structure of thermoelectric legs is essential, as their geometry affects the performance of devices. It has been reported that asymmetrical shape of thermoelectric legs can lead to a decrease in the thermal and electrical conductance, which in turn improve the Seebeck voltage due to an increase in the temperature difference [41]. In the present work, the temperature differences of the proposed asymmetrical legs are calculated by using the Fourier law. **Figure 1a** shows the proposed asymmetrical thermoelectric leg. For the sake of simplicity in the analysis, it is considered that such leg is constituted of four simpler geometrical legs connected thermally in parallel. By analyzing this simpler leg as shown in **Figure 1b**, it is possible to determine the temperature profile of the asymmetrical leg. Based on the Fourier law, the heat conduction along the simpler leg is defined by

$$\frac{dT}{dx} + \frac{\dot{Q}}{k}\left[\frac{L}{(mx+b)^2}\right] = 0 \tag{1}$$

Where, $\dot{Q}$ is the heat flux through the simpler leg, k is the thermal conductivity, $m = \tan(\theta)$ represents the slope of the pyramid, b is the half-length of the smaller cross section end, and L is the length of the sample. By solving Eq. (1) using the boundary conditions $T(x) = T_0$ at $x = x_0$, and considering the fact that four simpler legs in parallel to form a complete asymmetrical thermoelectric leg, the temperature profile of the thermoelectric leg of pyramidal shape is given by

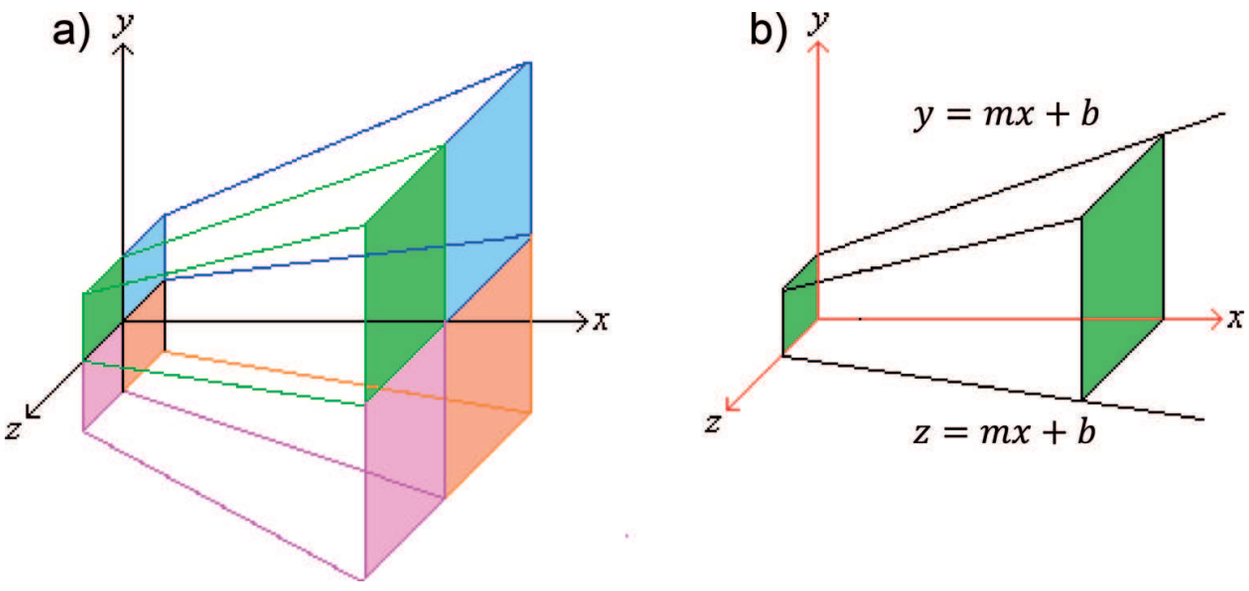

Figure 1. Schematic diagram of (a) a pyramidal-shaped thermoelectric leg and (b) simplified asymmetrical leg for modeling of the pyramidal-shaped thermoelectric legs.

$$T(x) = \frac{\dot{Q}}{4k}\left[\frac{L}{m(mx+b)}\right] - \frac{\dot{Q}}{4k}\left[\frac{L}{m(mx_0+b)}\right] + T_0 \tag{2}$$

Similarly, for a rectangular thermoelectric leg, the temperature profile is given by

$$T(x) = \frac{\dot{Q}L}{4k}\left[\frac{2x_0 - x}{a^2}\right] - \frac{\dot{Q}L}{4k}\left[\frac{x_0}{a^2}\right] + T_0 \tag{3}$$

where a is the half-length of the bigger cross-section end.

The thermoelectric modules experimentally analyzed in this chapter have rectangular thermoelectric legs based on Bi_2Te_3 with a typical dimension of around $1.7 \times 1.7 \times 2.1$ mm. Based on this dimensions and using Eqs. (2) and (3), **Figure 3a** shows the temperature profiles of an asymmetrical thermoelectric leg with a slant angle of 10° and a symmetrical thermoelectric leg under different heat fluxes, respectively. The upper solid lines (color online) represent the temperature profiles of the asymmetrical legs, whilst the lower dashed lines (color online) correspond to the temperature profiles of the symmetrical thermoelectric legs. As expected, as the heat flux decreases ($Q_1 > Q_2 > Q_3$), the temperature difference across the leg also decreases. Besides, a larger temperature difference is obtained across the asymmetrical leg as compared with the symmetrical one for a given heat flux. Therefore, by lowering the overall thermal conductance of the device via asymmetrical legs, the temperature gradient in the legs is increased, thus Seebeck voltage across terminals must be significantly increased. Besides, for simplicity it is worth to mention that the thermal conductivity k in Eqs. (2) and (3) during the modeling is taken as a constant, that is temperature independent; however, despite such simplification, uncertainty between both results is not so significant as it is seen in **Figure 2**. Hence, the main conclusions and results of the modeling are still valid.

Figure 3b shows the temperature profiles of the asymmetrical thermoelectric leg as a function of the position for different slant angles of the pyramid for a given heat flux. As expected, as the slant angle increases, the temperature difference across the leg increases; however, such increase is limited to a critical slant angle θ_c (see inset), at which a maximum temperature difference across the leg can be achieved without affect the leg length; such limit angle is given by

$$\tan(\theta_c) = \frac{a}{L} \tag{4}$$

Wherefrom, the limit angle for a thermoelectric leg with the length of 2.1 mm is around 22°, for this reason in **Figure 2b** as the slant angle achieves this value, the temperature rise increase drastically. It is worth to mention that in such modeling, convective effects were not taken into consideration because experimentally the device was tested under vacuum in order to avoid heat losses. Clearly, asymmetrical legs could help in two ways, by lowering the overall thermal conductance of the device so as to increase the temperature gradient in the legs, and by harnessing the Thomson effect, that depends on the temperature gradient in the legs and the temperature variation of Seebeck coefficient of the material in the operating temperature range, which is generally neglected in conventional rectangular thermoelectric legs. Thomson coefficient is given by $\tau(T) = TdS/dT$, when a temperature gradient is imposed on a thermoelectric material S varies from point to point along of the length of the thermoelectric element.

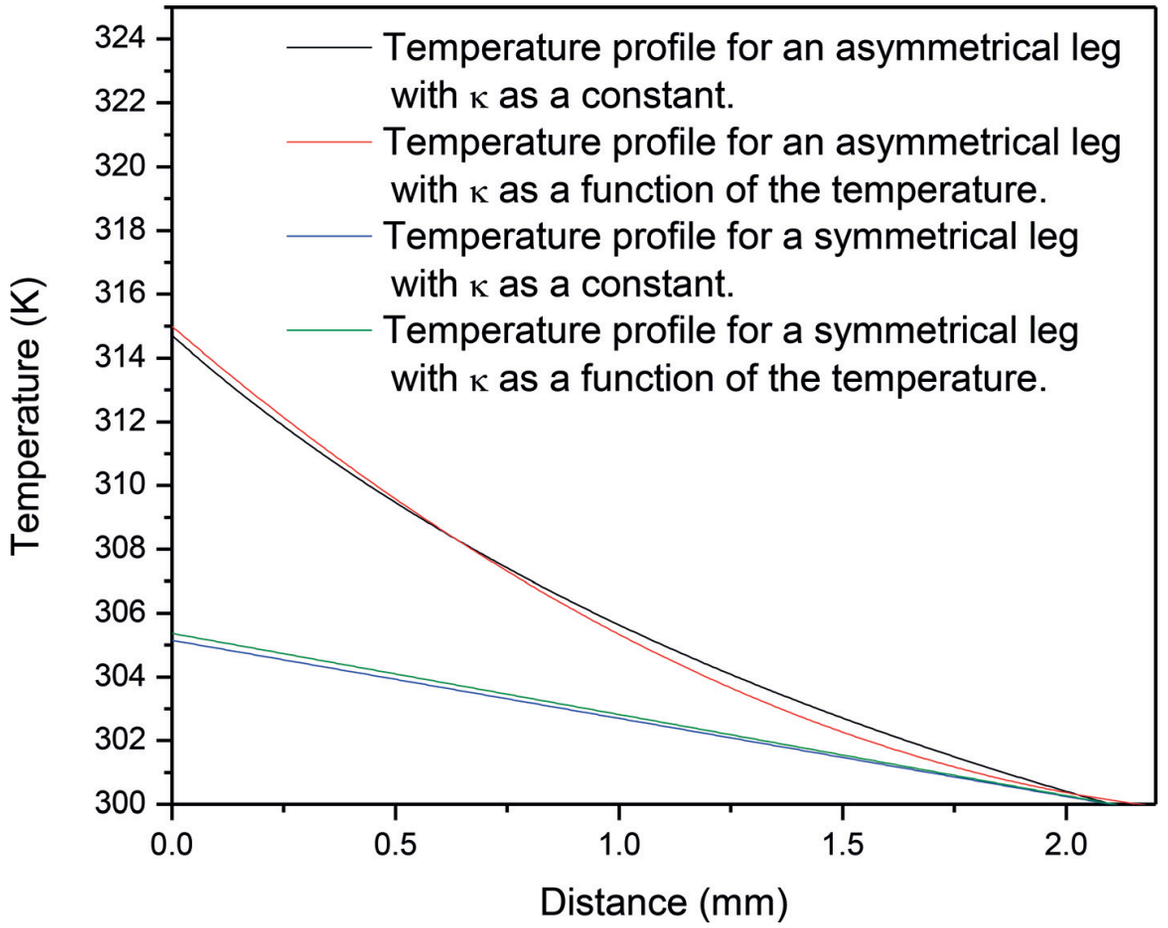

Figure 2. Comparison of temperature profiles taking κ as a function of the temperature as well as a constant, for symmetrical and asymmetrical thermoelectric legs.

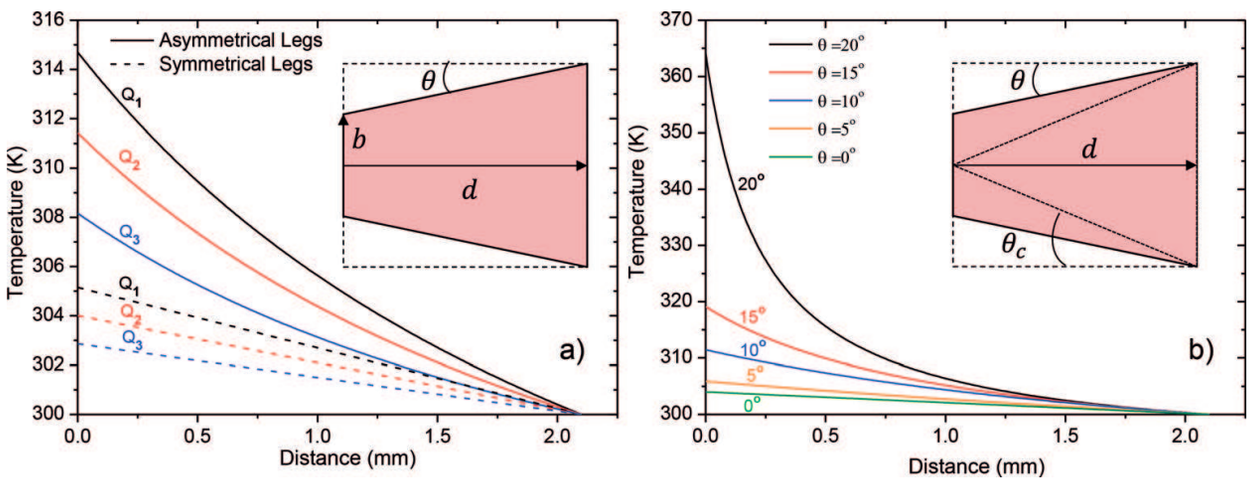

Figure 3. Temperature profiles as a function of the position for asymmetrical and rectangular thermoelectric legs at (a) different heat fluxes and at (b) different slant angle of the pyramid at room temperature.

The linear component in the temperature dependence of the intrinsic S can be taken into account so as to appear in the conventional thermal rate equations, but in fact it cancels out with the linear component of the Thomson coefficient and never appears in the thermal rate

http://dx.doi.org/10.5772/intechopen.75790

[equations 42]. Nevertheless, the nonlinear component in the temperature dependence of the intrinsic S has never been into consideration in the conventional thermal rate equations; thus when S varies nonlinearly with temperature, a portion of the nonlinear component of $\tau(T)$ remains in the thermal rate [equations 42]. Hence, when a thermoelectric element is subjected to a temperature gradient an effective Seebeck coefficient S_1 will appear. In this sense, previous experimental and analytical studies have demonstrated that an enhanced effective Seebeck coefficient can be obtained by combining the Thomson effect with the intrinsic Seebeck coefficient of a thermoelectric element because of the nonlinear changes in the intrinsic Seebeck coefficient with the temperature [43]. Hence, asymmetrical thermoelectric elements should present an enhancement in the effective Seebeck coefficient as compared to symmetrical ones because of the higher temperature gradient generated along the thermoelectric element as it is shown in **Figure 3a**.

Although in this chapter the influences of the temperature dependence of the thermal conductivity and Seebeck coefficient are not considered in the model given by Eqs. (2) and (3) for the sake of simplicity; however, the main conclusions arising from the model are still valid. In addition, a simulation study has been carried out using a finite element simulation on 3D geometries for a thermoelectric device consisting of nine pairs of pyramidal legs and rectangular legs respectively using the dedicated software "Thermoelectric module of COMSOL Multiphysics in Seebeck mode". **Figure 4a**, **b** show the simulation results of the temperature profiles and terminal voltages in the asymmetrical device respectively due to the presence of a given heat flux. For comparison, **Figure 4c**, **d** show the temperature profile and the terminal voltage in the symmetrical device respectively. Clearly, asymmetrical legs based thermoelectric device presents a higher open circuit terminal voltage than its rectangular counterpart as a consequence of the larger temperature difference generated in the legs because of their asymmetry.

The modules were made using p-type and n-Type Bi_2Te_3 thermoelectric materials available from Thermal Electronics Corp with ZT~1. For clarity, the full process so as to fabricate the thermoelectric legs is shown in **Figure 5**. The raw thermoelectric material in the form of a rod is covered by a layer of wax (wax-70) so as to hold the material in the cutting base during the cutting process, see **Figure 5a**. Then, it is cut into slices of 2.1 mm in thickness, which is the length of the thermoelectric leg as shown in **Figure 5b**. The wax is cleaned up using a warm solution of water and aquaclean-900 at a concentration of 10 mg/ml after slices cutting process as shown in **Figure 5c**. Next, a layer of Ni ranging from 0.5 and 1 μm is coated on both surfaces of the slide by electroplating. The Ni layer works as a diffusion barrier between the solder (Sn/Pb 60/40) and the thermoelectric legs, see **Figure 5d**. Prior to cutting, the Ni-electroplated slide is again fixed on a graphite plate using wax (wax-70) with the aim of keeping the legs during cutting, as you can see in **Figure 5e**. Subsequently, thermoelectric legs with the regular geometry of 1.7 × 1.7 × 2.1 mm are obtained using a circular saw cutting machine (Accutom-100), see **Figure 5f**. Finally, the wax is removed from legs as previously indicated in **Figure 5c**.

In order to obtain the asymmetrical legs, a similar process as described above is employed. However, in this case, a tilted base is used to hold the graphite plate during cuttings. Hence, so as to obtain the asymmetrical geometry (truncated square pyramid), it was necessary to do a

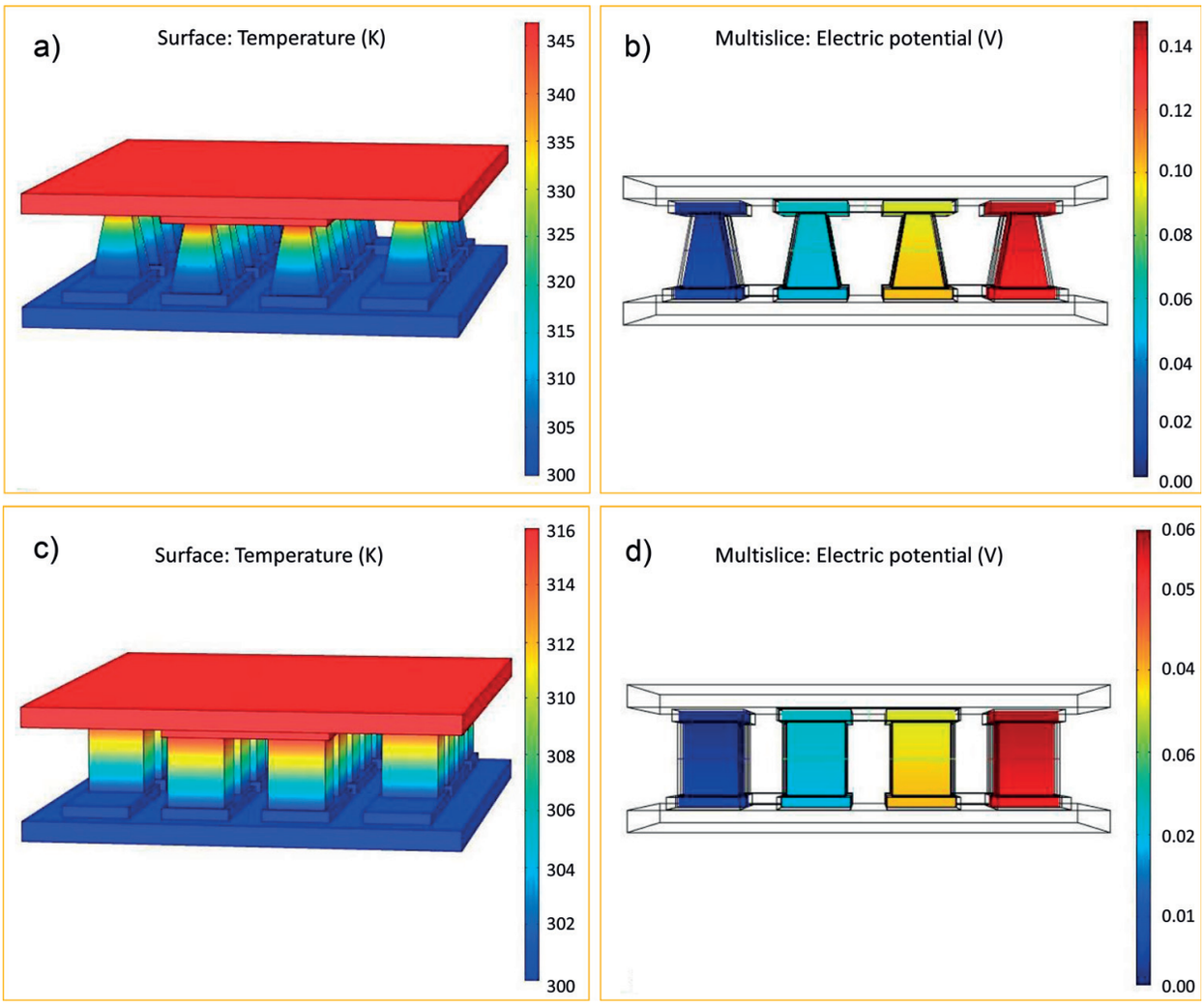

Figure 4. COMSOL simulation results: (a) temperature profile and (b) open circuit voltage for the asymmetrical thermoelectric module, (c) temperature profile and (d) open circuit voltage for the symmetrical thermoelectric module, respectively at room temperature.

cutting in every face of the rectangular leg by rotating the graphite tilted base 90° during each cutting. The slope of the base depends on the desired slant angle in the thermoelectric legs as shown in **Figure 6a**, **b**, clearly, the graphite plate is tilted at an angle of 10°. Besides, it has been attempted to fabricate the legs with a slant angle close to the critical angle of 22° so as to maximize the thermal gradient. However, it has been observed that angles higher than 10° produce legs with a small cross-section in the thin end. Such legs tend to be very fragile because of the mechanical properties of Bi_2Te_3, and they fracture during the assembling process due to the pressure and thermal treatments applied. **Figure 6c**, **d** show the side and top view of the asymmetrical legs used for the fabrication of the thermoelectric device.

Figure 7a, **b** show the images of the fabricated modules with symmetrical and asymmetrical legs, respectively, wherefrom differences in the geometry of the thermoelectric legs can be observed by comparing both images. At first instance, the performance of the devices has been evaluated by means of the hot-plate method. In such method, the thermoelectric modules are

http://dx.doi.org/10.5772/intechopen.75790

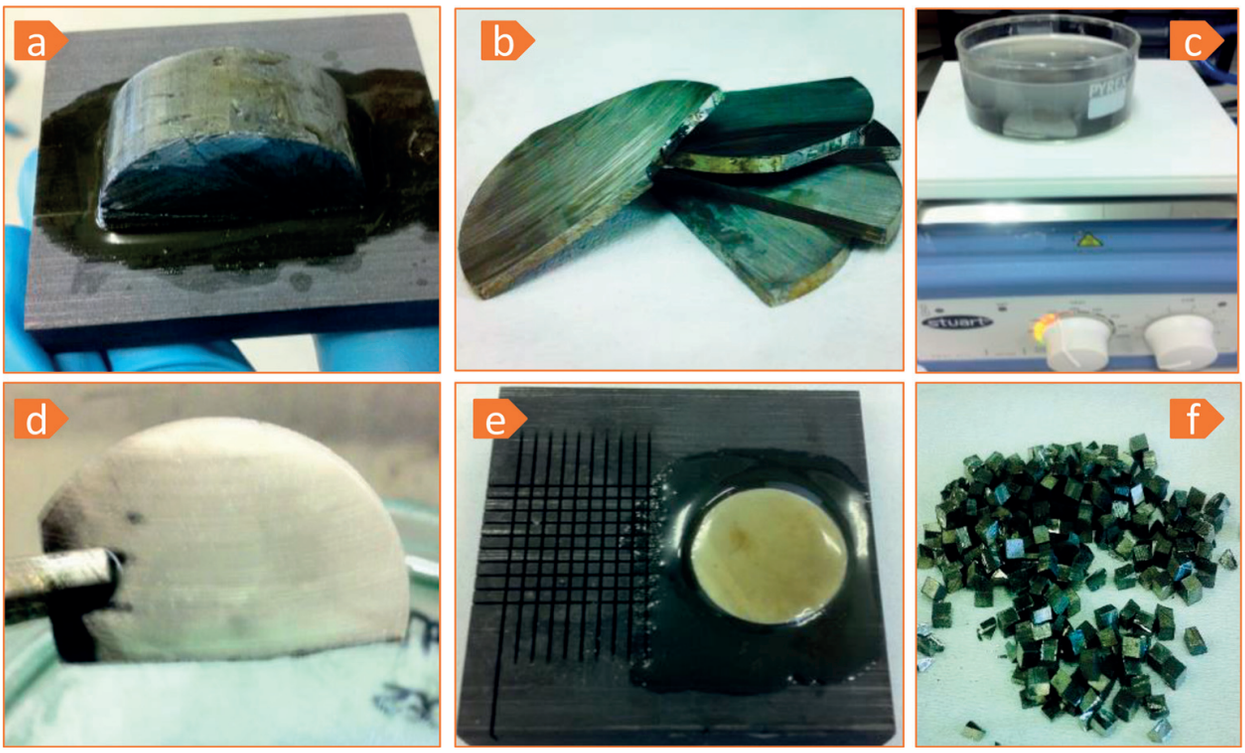

Figure 5. Steps for the fabrication of the thermoelectric legs.

installed between heating and cooling plates. Next, a dc voltage with regular increments is applied to the 130 Ω resistive heater of the heating plate by using the BK Precision 9184 dc power supply. This action induces a constant heat flow Q which flows through the test specimens in the stationary temperature state, as well as provides several temperature biases ΔT across the thermoelectric module surfaces. It is worth to note that the side of the applied heat source does not matter in symmetrical modules; however, in the asymmetrical module, the heat source must be applied necessarily on the smaller area side because it has the smallest thermal conductance along the pyramid. In **Figure 7c**, it is plotted ΔT vs Q wherefrom the slope it can be calculated the thermal resistance of the devices; evidently, the asymmetrical legs module presents a higher thermal resistance than the symmetrical legs module.

Parallel, the open circuit thermal voltage is measured along with the temperature rise across the device, such voltage is detected by using the Metrohm Autolab B. V. system; then, it is also plotted V vs Q as shown in **Figure 7d**. Again, the asymmetrical legs module presents a higher open circuit thermal voltage than its symmetrical counterpart; clearly, such enhancement must be related to the thermoelectric performance of the asymmetrical thermoelectric module. It is worth to mention that by continuing applying heat fluxes the temperature rise across the device will continue increasing, and therefore the open circuit output voltage also increases. However, if this heat flux becomes excessive, it could damage the device because of the melting of the weld joining the thermoelectric legs.

On the other hand, when a thermoelectric device is connected to any load it is desirable that such device be able to transfer the greatest amount of power to the load. In this sense, applying

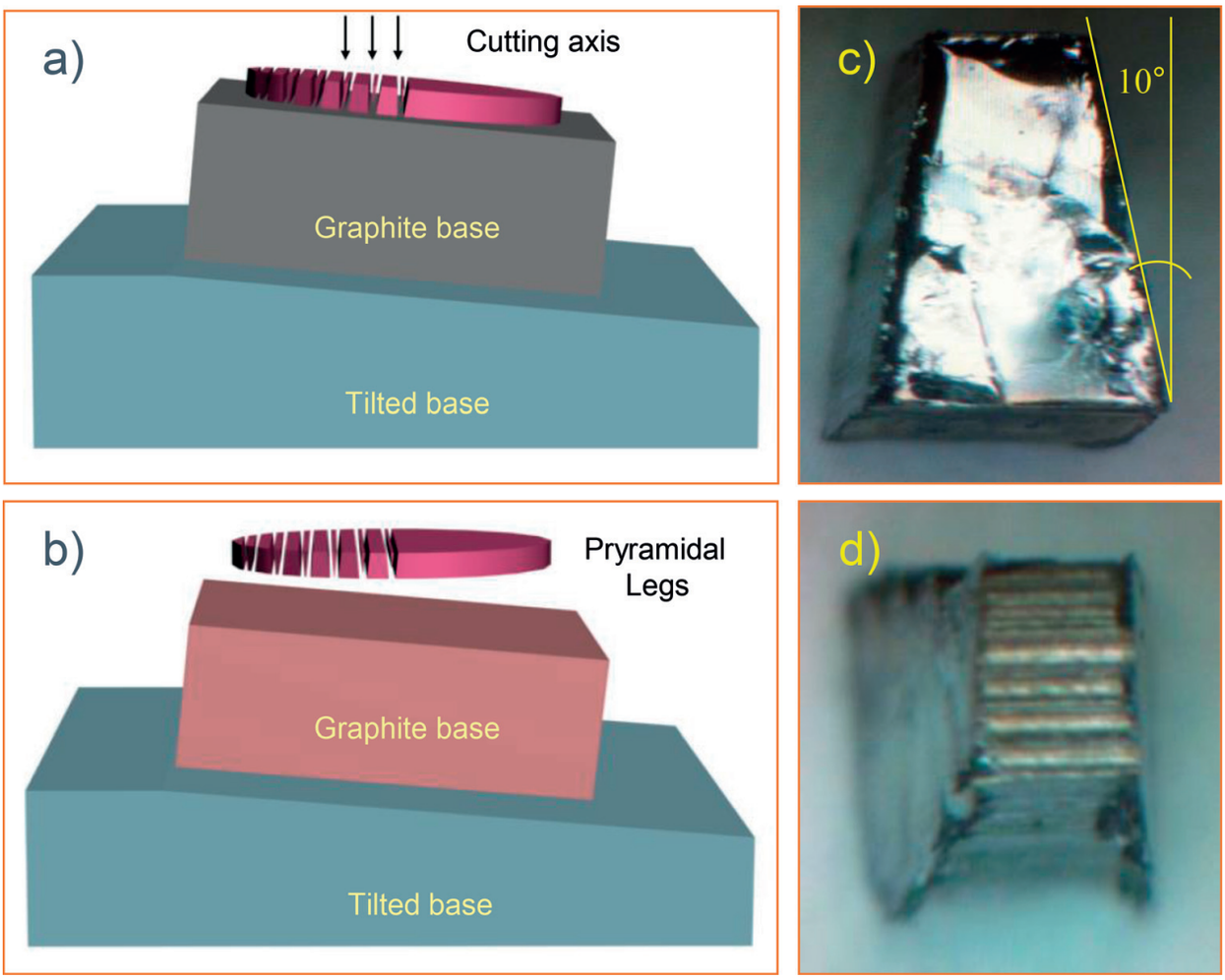

Figure 6. Schematic diagram of (a) the tilted base and (b) angled leg cutting suggested to obtain asymmetrical thermoelectric legs; micro-photographs of (c) side view and (d) top view of the thermoelectric legs.

the Theory of Maximum Power Transfer assumes a simple electrical circuit with a voltage source V which is the thermoelectric device; the source has an internal resistance R_i, a load resistance R_L, a voltage drop V_L, as shown in **Figure 8**.

The current is $I = V/(R_i + R_L)$ and the power delivered to the charge is

$$P = I^2 R_L = V^2 R_L/(R_L + R_i)^2 \tag{5}$$

Then is considered a variation in power when the load resistance R_L is changed, but internal resistance of thermoelectric device R_i as well as the voltage V are constants. When $R_L = 0$, the output power is clearly zero. Likewise, when R_L is too big, the output power is zero as well. This suggests that an intermediate value of R_L is maximum. When P is derived as a function of R_L in Eq. (5) and then it is equal to zero, it is easily shown that the maximum power is when $R_L = R_i$.

In this sense, in order to evaluate the maximum power given by the modules the maximum output power between the asymmetrical and the symmetrical modules has been evaluated by

http://dx.doi.org/10.5772/intechopen.75790

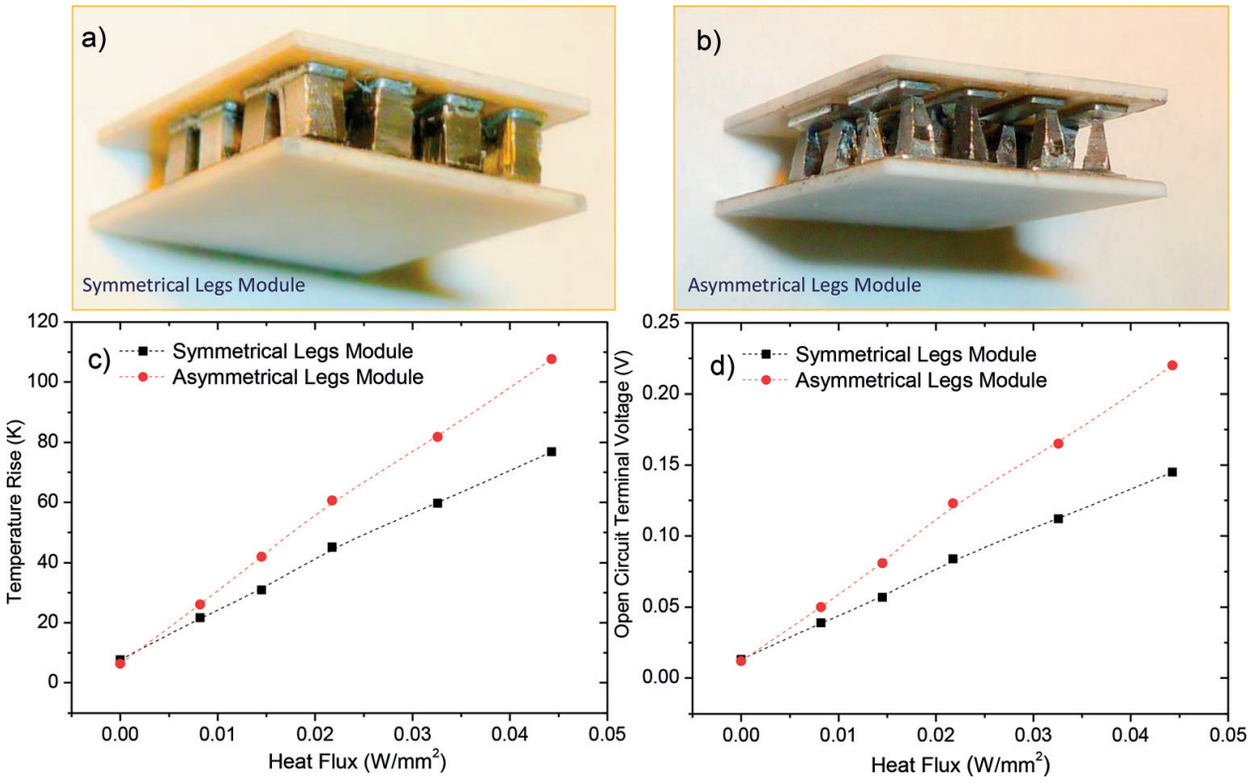

Figure 7. Photographs of the fabricated module of nine pairs of legs: (a) with symmetrical legs and (b) with asymmetrical legs; (c) temperature rise across both modules as a function of input heat flux; and (d) open circuit voltage as a function of input heat flux.

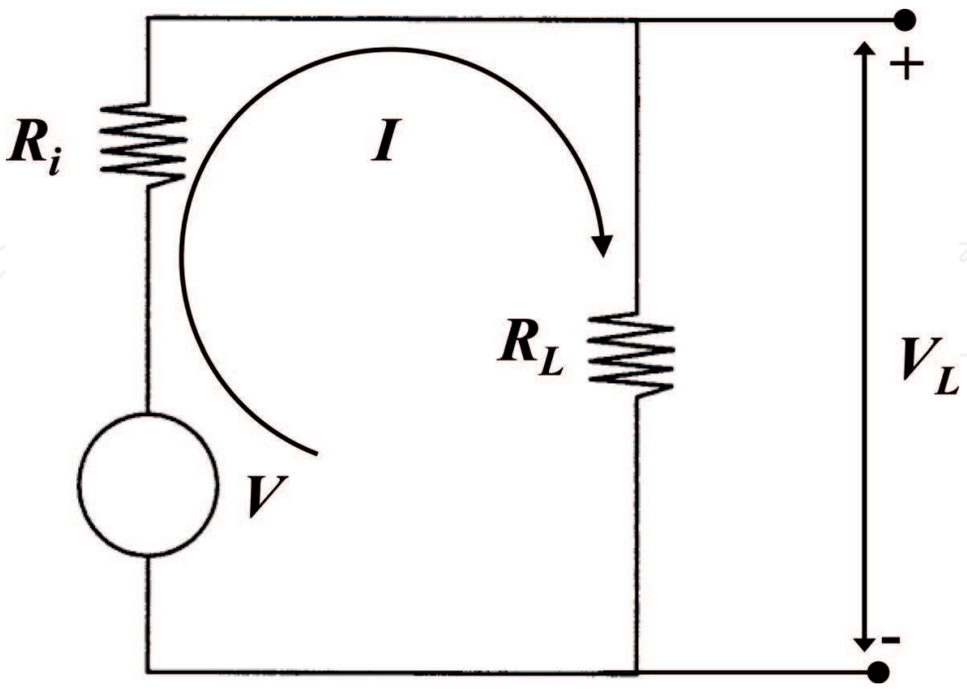

Figure 8. Basic electric circuit showing the internal resistance R_i of the thermoelectric device and the load resistance R_L.

way of the maximum power transfer theorem. In this case, an identical heat flux of around 4 mW/mm^2 was supplied to both modules by applying an electrical current of 90 mA to the Ohmic heater; once modules reached the steady state different load resistances were connected into the module and the voltage across the resistance was recorded, by using those voltages and resistances the output power was estimated. **Figure 9** shows the obtained results, it can be observed that asymmetrical module delivers more power than the symmetrical one once the load resistance equals the device internal resistance. In Fact, the asymmetrical thermoelectric module shows to have almost twofold the maximum delivered power as compared to conventional one with a constant square cross-section. Besides, by estimating the maximum available power per unit amount of material (mass of the legs) it has been obtained 433 μW/gram and 1.57 mW/gram for the symmetrical and the asymmetrical modules, respectively.

Evidently, these modules apparently present low output power, however by comparing these modules with several commercially available they have very competitive output power values [44]. For instance, by extrapolating the data shown in Ref. [44] to ΔT = 20°C a TEG module based on Bi_2Te_3 model FERROTEG 9501/71/040B with 71 pairs, and 22 mm × 22 mm generates a maximum output power around 1.5 mW. In our case, for modules with only nine pairs, we obtain 0.3 and 0.5 mW for symmetrical and asymmetrical modules, respectively. Nevertheless, by the projection of our modules to 71 pairs we would obtain 2.36 and 3.94 mW, respectively. Besides, if we compare our module against TEG-FERROTEG 9500/127/100B module based on Bi_2Te_3 with 127 pairs, and 40 × 40 mm under ΔT = 20°C, which delivers an output power around 2.5 mW, we would obtain by a similar extrapolation 4.23 and 7.05 mW for symmetrical and asymmetrical modules, respectively, under ΔT = 20°C. It is worth to mention that ΔT scale

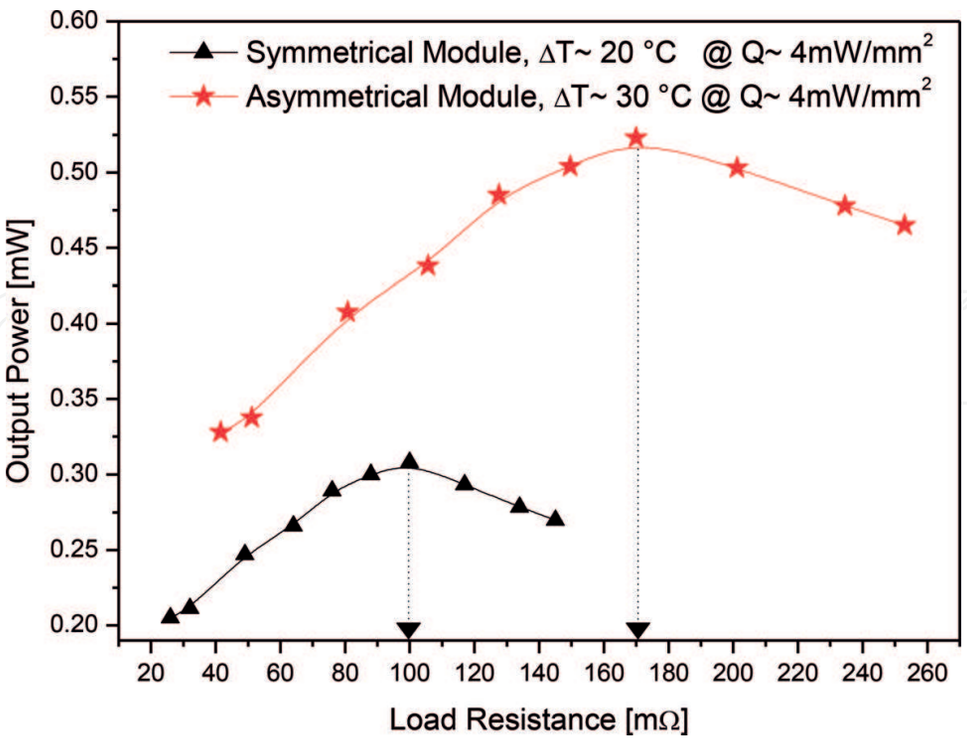

Figure 9. Output power vs load resistance for symmetrical and asymmetrical modules.

http://dx.doi.org/10.5772/intechopen.75790

in Ref. [44] is in logarithmic scale, so it can be closely compared to $\Delta T = 20^{\circ}C$ and $\Delta T = 30^{\circ}C$, for the asymmetrical module.

The thermoelectric figure of merit of the fabricated modules was also evaluated by using impedance spectroscopy technique [45]. In this method, the thermoelectric figure of merit is determined by measuring the adiabatic and isothermal responses of the module under electrical excitation. Under the adiabatic condition at steady state (i.e., $\omega = 0$), the total impedance of the module can be written as [45]

$$R_{ad} = R_{te} + R_{iso} \tag{6}$$

Where R_{te} is the thermoelectric resistance, and it refers to the resistance of the device which is the result of the temperature difference induced between the ends of the sample due to the Peltier effect, R_{iso} is the isothermal resistance, and it is the resistance of the device R_{iso} excluding thermal effects but including parasitic resistances such as contact and wire resistances, R_p.

According to the Harman method, the thermoelectric figure of merit is given by the ratio between the thermoelectric resistance and the isothermal resistance of the system [46]; hence, by dividing Eq. (6) by R_{iso}, ZT is calculated as a function of adiabatic resistance R_{ad}, isothermal resistance R_{iso}, and parasitic resistance R_p:

$$ZT = \frac{R_{ad} - R_p}{R_{iso} - R_p} - 1 \tag{7}$$

As well as, in terms of the thermoelectric resistance ZT is given by

$$ZT = \frac{R_{te}}{R_{iso} - R_p} \tag{8}$$

where

$$R_p = R_c + R_w \tag{9}$$

Therefore, by using Eqs. (7) or (8), the effective thermoelectric figure of merit of a device can be accomplished. The adiabatic and isothermal resistances can be easily accessed via electrical impedance measurements [45]. Likewise, parasitic resistances R_c from module with symmetrical and asymmetrical legs are evaluated by applying Transmission Line Method (TLM) [47] and so they can be removed from ZT as it seen in Eq. (7).

During the measurements, the samples were isolated and suspended to provide adiabatic conditions in a similar way as required in the Harman method [46]. **Figure 10a**, **b** show the experimental electrical impedance curves obtained for the symmetrical and asymmetrical leg modules, respectively. In both curves, the thermoelectric, adiabatic, and isothermal resistances are indicated in order to access to their respective values. Nevertheless, it is well known that a material has more than one contribution to its impedance response, which is often the case of thermoelectric materials where thermoelectric impedance, isothermal impedance, and contact impedance have distinct contributions. Hence, one can witness more than one semi-circle, often

overlapping each other which makes impossible to distinguish them. One of the ways to model such a behavior in a simple model can be using in three series–parallel RC elements circuit. In **Figure 10a**, **b**, the solid line corresponds to the obtained fitting results. For clarity, such resistance results, as well as the effective thermoelectric figure of merit of the symmetrical and asymmetrical modules are shown in **Table 1**. Evidently, the thermoelectric figure of merit of the asymmetrical module is almost two-fold the thermoelectric figure of merit of the symmetrical module, such result confirms the enhanced thermoelectric performance of the asymmetrical module as a consequence of the larger temperature rise generated in the legs because of their asymmetry. Hence, harnessing of the Thomson coefficient via asymmetrical legs could be an important strategy in order to accomplish thermoelectric devices with enhanced performance.

On the other hand, it is worth to mention that the present experimental research is mainly focused on the development of devices for applications at room temperature (i.e. 300 K), in that case, it is not necessary to measure the temperature dependence of ZT. Besides, our devices are based on P and N-type Bi_2Te_3, it is well known that such materials present an optimal thermoelectric performance at around room temperature; hence, operation of such materials must be well below 100°C, so an operation condition above this temperature will damage the device because by applying an excessive heat flux it could damage the device due to the melting of the weld joining the thermoelectric legs. In this sense, it is not possible to operate such device under a high-temperature rise away from room temperature would affect seriously their performance.

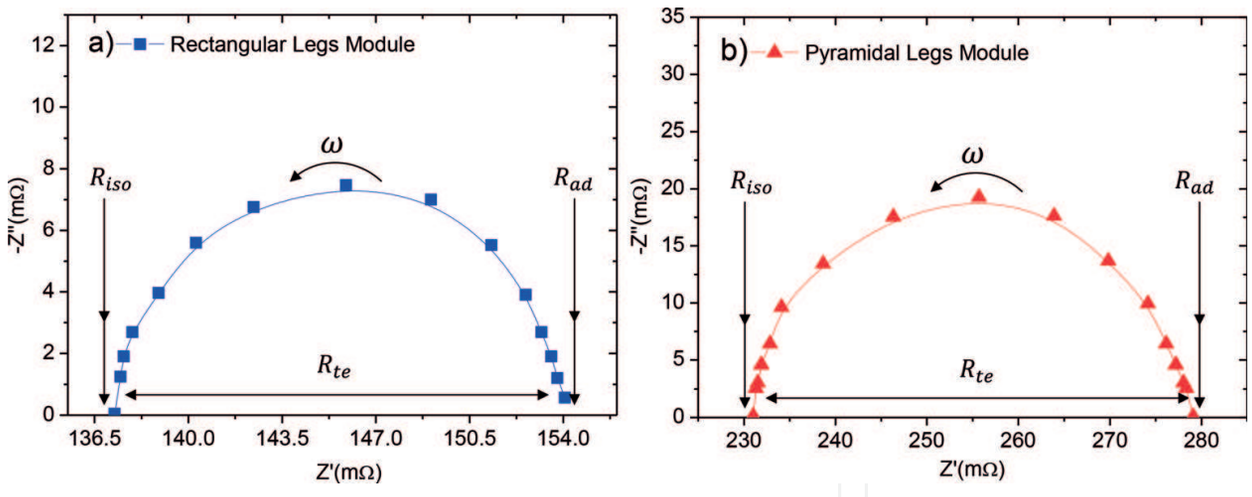

Figure 10. Experimental electrical impedance curves at room temperature for (a) symmetrical and (b) asymmetrical nine pairs of thermoelectric modules.

Module	R_{iso}(mΩ)	R_{te}(mΩ)	R_{ad}(mΩ)	R_c(mΩ)	R_w(mΩ)	ZT_c
Symmetrical	137.25	16.81	154.06	98.2	18.3	0.43
Asymmetrical	231.01	48.09	279.10	165.4	18.3	0.73

Table 1. Experimental parameters of the symmetrical and asymmetrical leg thermoelectric modules.

http://dx.doi.org/10.5772/intechopen.75790

Moreover, according to the values shown in **Table 1**, evidently, the parasitic electrical resistances play an important role in the performance of the device. For instance, if we take into consideration only parasitic contact effects (i.e. parasitic electrical contact resistance between legs and ceramic plates) and neglect the effect of parasitic resistances generated by cable wiring, a value of 0.43 and 0.73 on *ZT* is obtained.

3. Impact of parasitic contact electrical resistances on *ZT* of the thermoelectric device

Thermoelectric device engineering involves the formation of several intrinsic parasitic resistances that affect the thermoelectric module performance. In this sense, the TLM has been applied to discard the parasitic resistances and demonstrate that the increase on *ZT* of the device is mainly due to asymmetric effect in thermoelectric legs and consequently the nonlinear Thomson effect that governs them.

Figure 11a shows different lengths in the symmetrical and asymmetric thermoelectric legs as well as their respective electrical resistances as a function of length. The total measured resistance consists of several components:

$$R_T = R_{W1} + R_{C1} + R_{p-TE} + R_{C2} + R_{n-TE} + R_{C3} + R_{W2} \tag{10}$$

Where R_{W1} y R_{W2} are wiring resistances, R_{C1} y R_{C3} are contact resistances due to metal contacts, R_{C2} is associated with the metallic contact between the junction of the P-type and N-type thermoelectric legs, and $R_{P\text{-}TE}$ and $R_{N\text{-}TE}$ define the internal resistance of the P-type and N-type thermoelectric legs, respectively.

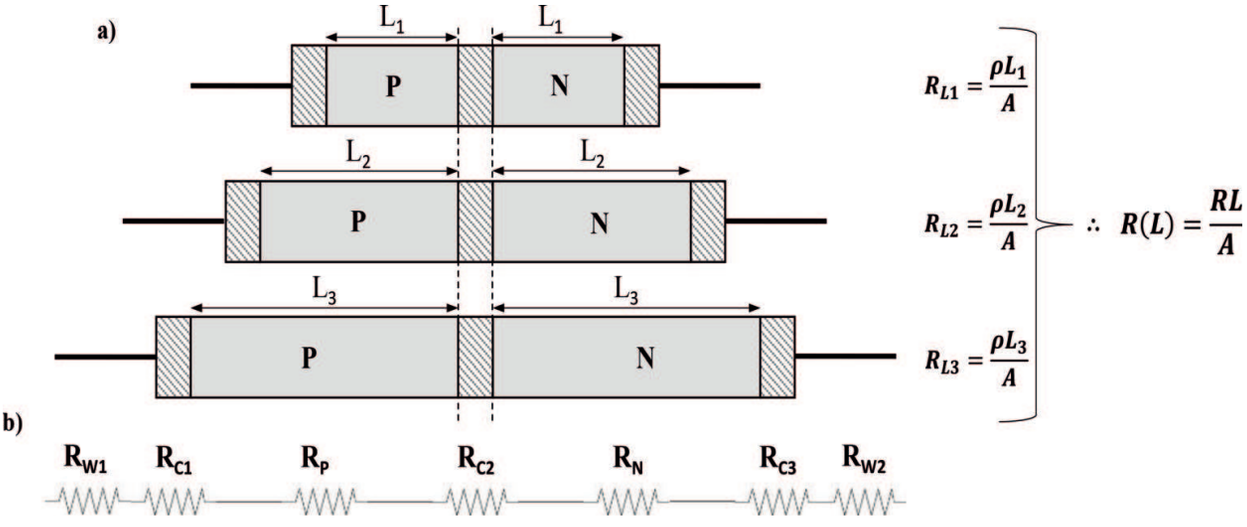

Figure 11. (a) Diagram of the variation of the length in thermoelectric couples and analysis of the electrical resistance, and (b) analogous electrical circuit of thermally coupled pairs with welding.

Therefore, the total parasitic electrical resistance Rp is given by the contact resistance Rc and the wiring resistance Rw, then Eq. (10) can be rewritten as:

$$R_p = R_w + R_c \tag{11}$$

By way of the TLM, it is possible to measure the total parasitic electrical resistance Rp. In this sense, thermoelectric legs have been fabricated with 2, 3, and 4 mm in length. The TLM is a technique used to determine the contact resistance between a metal and a semiconductor. First, the electrical resistance is measured for each length and then each resistance is presented as a function of length as shown in **Figure 12**. In the limit of a zero-length resistor, the residual resistance would be just the contact resistance. Then can be found from the graph by extrapolating back to L = 0. Then, the parasitic resistance of the P-N junction is the sum of such interceptions; hence, the total parasitic resistance of the device is estimated by multiplying this value by the number of P-N junctions in the device (in this case, 9 P-N pairs).

The total parasitic resistance *Rp* of a thermoelectric module with nine couples of symmetrical legs (see **Figure 7a**) is calculated as:

$$R_{p-symmetric} = (R_{c-P} + R_{c-N}) * 9$$

$$R_{p-symmetric} = (10.23m\Omega + 2.22m\Omega) * 9$$

$$R_{p-symmetric} = 115.29\ m\Omega$$

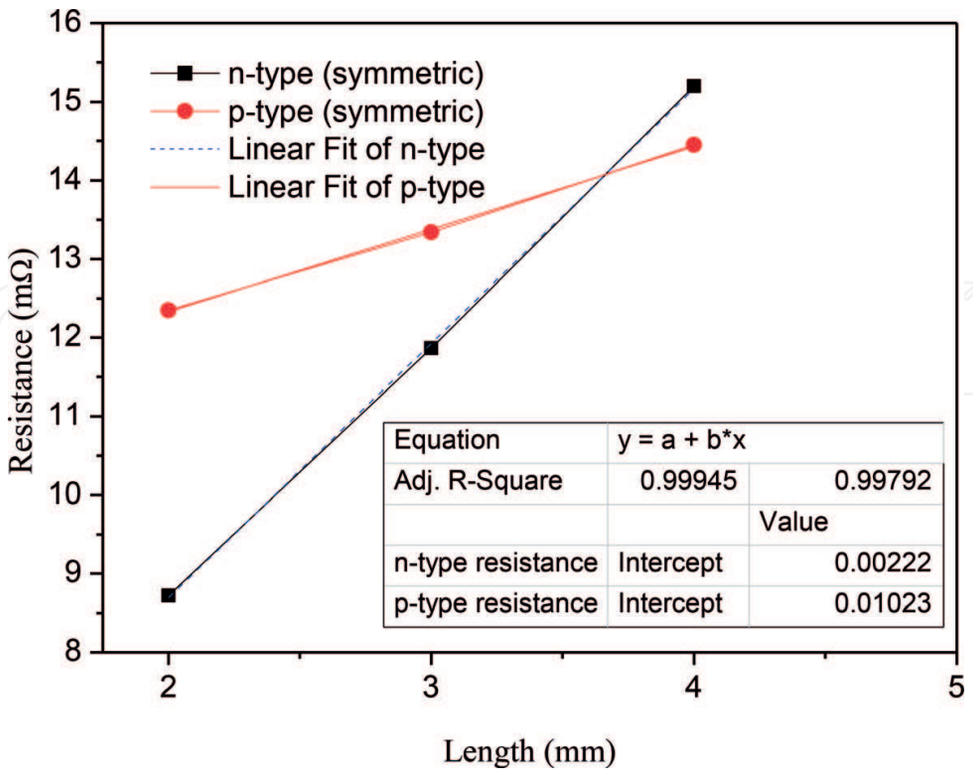

Figure 12. Electrical resistance in symmetrical thermoelectric legs as the length is increased.

Where, R_{c-P} y R_{c-N} values are defined by slope interception with y-axes, as mentioned above. Such values are shown as inset table of **Figure 12**. This result is the total parasitic resistance of thermoelectric module with nine pairs that includes the wiring resistance of wire used during measurements as well as contact resistance.

In addition, by way of the four-probe AC method, it is possible to measure the wiring resistance *Rw*, as shown in **Figure 13**. Where the value *Rw* is obtained by the intersection of the adjustment with the *y*-axis as it is shown in the inset.

Now, contact resistance Rc of the thermoelectric module with symmetrical legs is calculated as:

$$R_C = R_{p-symmetric} - R_W$$

$$R_C = 115.29\ m\Omega - 18.38\ m\Omega$$

$$R_{C-symmetric} = 96.91\ m\Omega$$

By applying a similar procedure, it is possible to measure the parasitic resistance Rp using the TLM in the asymmetric device, in this case, the resistance as a function of the length is shown in **Figure 14**.

The total parasitic resistance *Rp* of a thermoelectric module with nine couples of asymmetrical legs (see **Figure 7b**) is calculated as:

$$R_{p-asymmetric} = (R_{c-P} + R_{c-N}) * 9$$

$$R_{p-asymmetric} = (17.84 m\Omega + 3.59 m\Omega) * 9$$

$$R_{p-asymmetric} = 191.97\ m\Omega$$

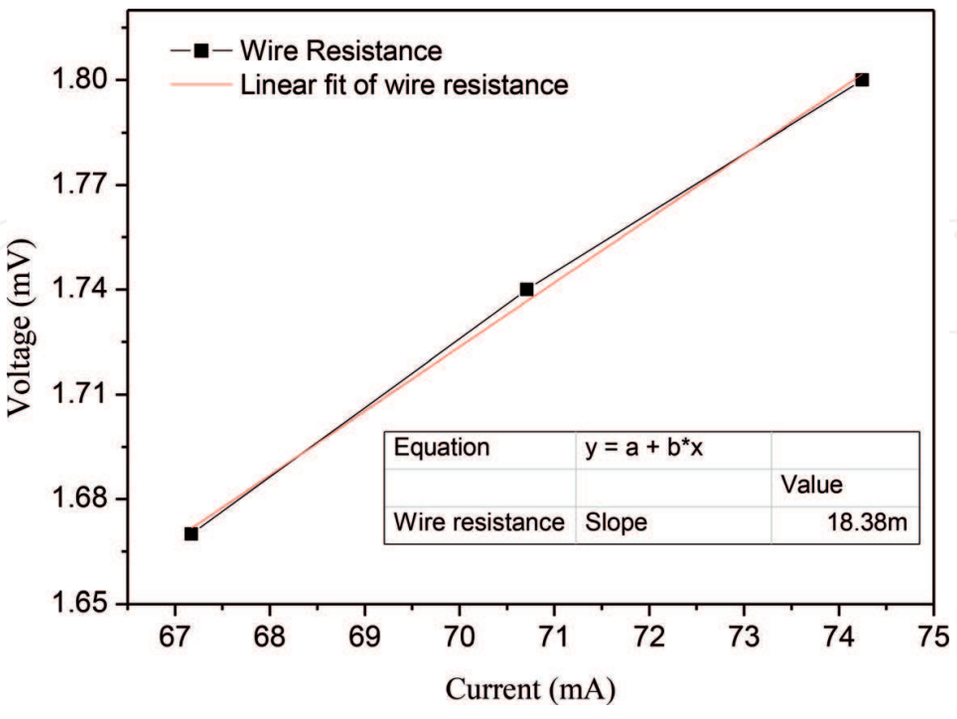

Figure 13. Wiring resistance of the wire used during thermoelectric characterization.

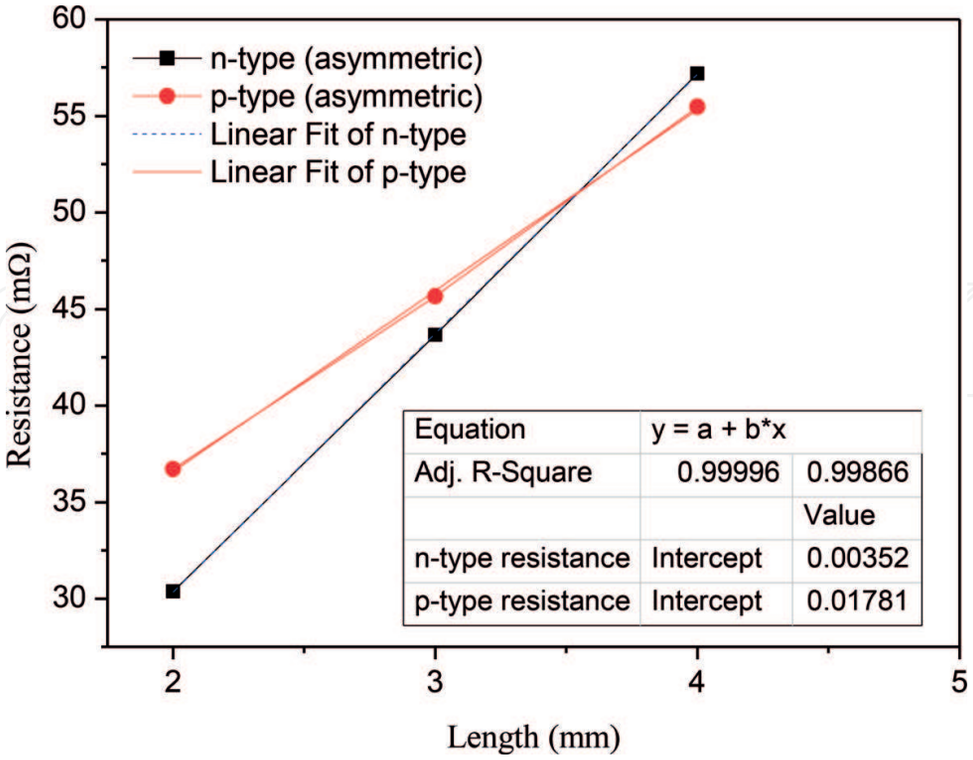

Figure 14. Electrical resistance in asymmetrical thermoelectric legs as the length is increased.

Where, R_{c-P} y R_{c-N} values are defined by slope interception with y axes. Such values are shown as inset table of **Figure 14**. This result is the total parasitic resistance of thermoelectric module with nine pairs of asymmetrical legs that includes the wiring resistance of wire used during measurements as well as contact resistance.

Now, contact resistance R_c of the thermoelectric module with asymmetrical legs is calculated as:

$$R_C = R_{p-asymmetric} - R_W$$

$$R_C = 191.97\ m\Omega - 18.38\ m\Omega$$

$$R_{C-asymmetric} = 174\ m\Omega$$

In this particular case, R_p has been obtained around 116 mΩ y 183 mΩ for the symmetrical and asymmetrical device, respectively. Using this information, ZTp can be calculated as it is shown in **Table 2**. However, by correcting such parasitic effects the estimated values on ZT_p are 0.79 and 1.02 for the symmetrical and asymmetrical thermoelectric modules, respectively. Thus, it is

Module	ZT_c	ZT_p
Symmetric	0.43	0.79
Asymmetric	0.73	1.02

Table 2. Effect of contact and parasitic resistances on ZT of thermoelectric modules with symmetrical and asymmetrical legs, respectively.

demonstrated that clearly parasitic electric resistance plays an important role in the performance of the thermoelectric device.

4. Conclusion

In the present chapter, it has been done an experimental demonstration of the influence of the device legs geometry as well as parasitic electrical contact resistance on ZT. Results prove that asymmetrical thermoelectric module shows to have almost twofold the thermoelectric figure of merit as compared to conventional one with a constant square cross-section. Thermal analysis of the device via analytical, as well as numerical modeling unveils an increment in the temperature gradient and Seebeck voltage across the device with asymmetrical thermoelectric legs. Such result confirms that the thermoelectric enhancement is due to the harnessing of Thompson effect which is normally neglected in rectangular legs devices. Additionally, the impact of parasitic electrical contact and wiring resistances on the thermoelectric module performance is shown. In this sense, a significant decrement on ZT due to parasitic effects is observed. Thereby, the general results of the present chapter experimentally prove that geometrical configuration of the device legs can improve significantly the thermoelectric performance of the device opening a new route to the development of enhanced performance thermoelectric modules via device engineering.

Acknowledgements

This work was supported by the National Council for Science and Technology-Conacyt Mexico, through the Grant for fundamental research No. 241597 and national issues No.1358. A.F. M. thanks to Conacyt Mexico for fellowship, as well as the thermoelectric laboratory at the Cardiff University for facilities.

Conflict of interest

Authors declare no conflicts of interest.

Author details

Angel Fabiam-Mijangos[1] and Jaime Alvarez-Quintana[1,2]*

*Address all correspondence to: jaime.alvarez@cimav.edu.mx

1 Centro de Investigación en Materiales Avanzados S. C. Unidad Monterrey, Apodaca, Nuevo León, México

2 Genes-Group of Embedded Nanomaterials for Energy Scavenging, CIMAV-Unidad Monterrey, Apodaca, Nuevo León, México

References

[1] Tritt TM, Subramanian MA. Thermoelectric materials, phenomena, and applications: A bird's eye view. MRS Bulletin. 2016;**31**(3):188. DOI: 10.1557/mrs2006.44

[2] Pop E. Energy dissipation and transport in nanoscale devices. Nano Research. 2010;**3**:147-169

[3] Wang S, Fu F, She X, Zheng G, Li H, Tang X. Optimizing thermoelectric performance of Cd-doped β-Zn4Sb3 through self-adjusting carrier concentration. Intermetallics. 2011;**19**: 1823-1830

[4] Dresselhaus MS, Chen G, Tang MY, Yang RG, Lee H, Wang DZ, et al. New directions for low-dimensional thermoelectric materials. Advanced Materials. 2007;**19**:1043-1053

[5] Hicks LD, Dresselhaus MS. Thermoelectric figure of merit of a one-dimensional conductor. Physical Review B. 1993;**47**:16631-16634

[6] Hicks LD, Dresselhaus MS. Effect of quantum-well structures on the thermoelectric figure of merit. Physical Review B. 1993;**47**:12727-12731

[7] Chen G, Dresselhaus MS, Dresselhaus G, Fleurial J-P, Caillat T. Recent developments in thermoelectric materials. International Materials Review. 2003;**48**:45-66

[8] Snyder GJ, Toberer ES. Complex thermoelectric materials. Nature Materials. 2008;**7**:105-114

[9] Venkatasubramanian R, Siivola E, Colpitts T, O'Quinn B. Thin-film thermoelectric devices with high room-temperature figures of merit. Nature. 2001;**413**:597-602

[10] Sun X, Zhang Z, Dresselhaus MS. Theoretical modeling of thermoelectricity in Bi nanowires. Applied Physics Letters. 2016;**4005**:26-29

[11] Zhu T, Ertekin E. Phonon transport on two-dimensional graphene/boron nitride superlattices. Physical Review B. 2014;**90**:195209

[12] Chen Z-G, Han G, Yang L, Cheng L, Zou J. Nanostructured thermoelectric materials: Current research and future challenge. Progress in Natural Science: Materials International. 2012;**22**:535-549

[13] Poudel B, Hao Q, Ma Y, Lan Y, Minnich A, Yu B, et al. High-thermoelectric performance of nanostructured bismuth antimony telluride bulk alloys. Science. 2008;**320**:634-638

[14] Oh T-S. Thermoelectric characteristics of p-type (Bi,Sb)2Te3/(Pb,Sn)Te functional gradient materials with variation of the segment ratio. Journal of Electronic Materials. 2009;**38**(7):1041

[15] Vining CB. An inconvenient truth about thermoelectrics. Nature Materials. 2009;**8**:83-85

[16] Hsu FK. Cubic AgPbmSbTe2+m: Bulk thermoelectric materials with high figure of merit. Science. 2004;**303**:818-821

[17] Zhao XB, Ji XH, Zhang YH, Zhu TJ, Tu JP, Zhang XB, et al. Bismuth telluride nanotubes and the effects on the thermoelectric properties of nanotube-containing nanocomposites. Applied Physics Letters. 2016:062111

[18] Ni HL, Zhao XB, Zhu TJ, Ji XH, Tu JP. Synthesis and thermoelectric properties of Bi2Te3 based nanocomposites. Journal of Alloys and Compounds. 2005;**397**:317-321

[19] Slack GA, Hussain MA. The maximum possible conversion efficiency of silicon-germanium thermoelectric generators. Journal of Applied Physics. 2016;**2694**

[20] Kim W, Zide J, Gossard A, Klenov D, Stemmer S, Shakouri A, et al. Thermal conductivity reduction and thermoelectric figure of merit increase by embedding nanoparticles in crystalline semiconductors. Physical Review Letters. 2006;**96**:45901

[21] Alvarez-Quintana J. Impact of the substrate on the efficiency of thin film thermoelectric technology. Applied Thermal Engineering. 2015;**84**:206-210

[22] Salvador JR, Cho JY, Ye Z, Moczygemba JE, Thompson AJ, Sharp JW, et al. Conversion efficiency of skutterudite-based thermoelectric modules. Physical Chemistry. 2014;**16**: 12510-12520

[23] Taguchi K, Terakado K, Ogusu M, Matumoto A, Kayamoto T, Okura K, et al. Linear shaped Si-Ge thermoelectric module. In: Reference Number F2000A045 in Proceedings of Seul 2000 FISITA World Automotive Congress; 2000. pp 1-5

[24] Joshi G, He R, Engber M, Samsonidze G, Pantha T, Dahal E, et al. NbFeSb-based p-type half-Heuslers for power generation applications. Energy & Environmental Science. 2014;**7**:4070-4076

[25] Fujisaka T, Sui H, Suzuki RO. Design and numerical evaluation of Cascade-type thermoelectric modules. Journal of Electronic Materials. 2013;**42**:1688-1696

[26] Sun T, Peavey JL, David Shelby M, Ferguson S, O'Connor BT. Heat shrink formation of a corrugated thin film thermoelectric generator. Energy Conversion and Management. 2015; **103**:674-680

[27] Madan D, Chen A, Wright PK, Evans JW. Printed Se-doped MA n-type Bi2Te3 thick-film thermoelectric generators. Journal of Electronic Materials. 2012;**41**(6):1481

[28] Chen A, Madan D, Wright PK, Evans JW. Dispenser-printed planar thick-film thermoelectric energy generators. J Micromechanics Microengineering. 2011;**104006**:21

[29] Zheng XF, Liu CX, Yan YY, Wang Q. A review of thermoelectrics research – Recent developments and potentials for sustainable and renewable energy applications. Renewable and Sustainable Energy Reviews. 2014;**32**:486-503

[30] Aswal DK, Basu R, Singh A. Key issues in development of thermoelectric power generators: High figure-of-merit materials and their highly conducting interfaces with metallic interconnects. Energy Conversion and Management. 2016;**114**:50-67

[31] Hamid Elsheikh M, Shnawah DA, Sabri MFM, Said SBM, Haji Hassan M, Ali Bashir MB, et al. A review on thermoelectric renewable energy: Principle parameters that affect their performance. Renewable and Sustainable Energy Reviews. 2014;**30**:337-355

[32] Fateh H, Baker CA, Hall MJ, Shi L. High fidelity finite difference model for exploring multi-parameter thermoelectric generator design space. Applied Energy. 2014;**129**:373-383

[33] Hodes M. Optimal pellet geometries for thermoelectric power generation. IEEE Trans Components Packag Technol. 2010;**33**:307-318

[34] Sahin AZ, Yilbas BS. The thermoelement as thermoelectric power generator: Effect of leg geometry on the efficiency and power generation. Energy Conversion and Management. 2013;**65**:26-32

[35] Shi Y, Mei D, Yao Z, Wang Y, Liu H, Chen Z. Nominal power density analysis of thermoelectric pins with non-constant cross sections. Energy Conversion and Management. 2015;**97**:1-6

[36] Yilbas BS, Ali H. Thermoelectric generator performance analysis: Influence of pin tapering on the first and second law efficiencies. Energy Conversion and Management. 2015;**100**: 138-146

[37] Ali H, Sahin AZ, Yilbas BS. Thermodynamic analysis of a thermoelectric power generator in relation to geometric configuration device pins. Energy Conversion and Management. 2014;**78**:634-640

[38] Xuan XC, Ng KC, Yap C, Chua HT. Optimization of two-stage thermoelectric coolers with two design configurations. Energy Conversion and Management. 2002;**43**:2041-2052

[39] Cheng Y-H, Lin W-K. Geometric optimization of thermoelectric coolers in a confined volume using genetic algorithms. Applied Thermal Engineering. 2005;**25**:2983-2997

[40] Cheng Y-H, Shih C. Maximizing the cooling capacity and COP of two-stage thermoelectric coolers through genetic algorithm. Applied Thermal Engineering. 2006;**26**:937-947

[41] Mu Y, Chen G, Yu R, Li G, Zhai P, Li P. Effect of geometric dimensions on thermoelectric and mechanical performance for Mg2Si-based thermoelectric unicouple. Materials Science in Semiconductor Processing. 2014;**17**:21-26

[42] Ioffe AF. Semiconductor thermoelements and thermoelectric cooling. Infosearch London. 1957

[43] Yamashita O. Resultant Seebeck coefficient formulated by combining the Thomson effect with the intrinsic Seebeck coefficient of a thermoelectric element. Energy Conversion and Management. 2009;**50**(9):2394

[44] Salerno D. Ultralow voltage energy harvester uses thermoelectric generator for battery-free wireless sensor. Journal of Analog Innovation. 2010;**20**(3):1

[45] García-cañadas J, Min G. Impedance spectroscopy models for the complete characterization of thermoelectric materials. Journal of Applied Physics. 2014;**116**:174510

[46] Iwasaki H, Koyano M, Hori H. Evaluation of the figure of merit on thermoelectric materials by Harman method. Japanese Journal of Applied Physics. 2002;**41**:6606

[47] Reeves GK, Harrison HB. Obtaining the specific contact resistance from transmission line model measurements. IEEE Electron Device Letters. 1982;**3**:111-113